Conceptual Design of a Liquid Metal Limiter/Divertor System for the FFHR-d1

J. Miyazawa[1,2], T. Goto[1,2], T. Murase[1], T. Ohgo[2], N. Yanagi[1,2], H. Tanaka[3], H. Tamura[1], T. Tanaka[1,2], S. Masuzaki[1], R. Sakamoto[1,2], J. Yagi[1,2], A. Sagara[1,2], and the FFHR Design Group

[1]National Institute for Fusion Science, 322-6 Oroshi, Toki, Gifu 509-5292, Japan
[2]SOKENDAI (The Graduate University for Advanced Studies), 322-6 Oroshi, Toki, Gifu 509-5292, Japan
[3]Nagoya University, Furo-cho, Chikusa-ku, Nagoya, Aichi 464-8603, Japan
E-mail: miyazawa@LHD.nifs.ac.jp

Abstract

A new liquid metal divertor system named the REVOLVER-D (Reactor-oriented Effectively VOLumetric VERtical Divertor) is proposed for the helical fusion reactor FFHR-d1. The REVOLVER-D is composed of molten tin shower jets stabilized by internal flow resistances of wire/tape/chain. These shower jets are inserted to the ergodic layer surrounding the main plasma. Tin is selected as the liquid metal because of its low melting point, low vapor pressure, low material cost, and high safety. The liquid metal pumps, cryopumps, and turbo molecular pumps are installed in the central vacuum vessel connected to the main vacuum vessel via 10 inner ports equipped with maze neutron shields. Central solenoid coils made of high-temperature superconductors are installed inside the central vacuum vessel to shield the pumps from the strong magnetic field. The REVOLVER-D has a good possibility to satisfy important characteristics required for the divertor system in a fusion reactor, *i.e.*, high heat load tolerance, high maintainability, ~~enough~~ sufficient vacuum pump speed, high level of safety, and a small amount of radioactive wastes.

Keywords: liquid metal, divertor, high heat load, particle control, vacuum pumping, fusion reactor, heliotron

---

1. Introduction

Conceptual design activity of a helical fusion reactor FFHR-d1 is ongoing [1,2]. In designing the divertor system for FFHR-d1, special emphasis is placed on five issues, *i.e.*, high heat load tolerance, high maintainability, ~~enough~~ sufficient vacuum pump speed, high level of safety, and a small amount of radioactive wastes. To satisfy these requirements, a new concept of limiter/divertor consisting of liquid metal shower jets has been proposed and named the REVOLVER-D (Reactor-oriented Effectively VOLumetric VERtical Divertor).

The FFHR-d1 is a heliotron-type fusion reactor, of which the arrangement of superconducting magnetic coils is similar to that in the Large Helical Device (LHD) [3]. The device size is four times larger than the LHD. The major radius of the helical coil center is 15.6 m, the magnetic field strength is > 5 T at the plasma center, and the fusion output is ~3 GW [1,2]. The FFHR-d1 is inherently equipped with a helical divertor as is the LHD [4]. Compared with the conventional poloidal divertor in tokamaks, the helical divertor is characterized by a large plasma-wetted area spreading over both toroidal and poloidal directions. For example, the typical plasma-wetted area in LHD is estimated to be ~2 m^2 [5]. Since the footprint of the helical divertor is basically determined by the distribution of magnetic field lines of force, the plasma-wetted area in FFHR-d1 can be estimated as ~2 × 4 × 4 ~ 32 m^2, as long as the divertor plates are similarly placed in these two devices. If there is no radiation loss in FFHR-d1 and all of the alpha heating power of 600 MW hits the divertor in steady-state, then the averaged divertor heat flux becomes ~20 MW/m^2. This can be largely reduced by enhancing the radiation loss and realizing "divertor detachment" [6]. However, it will be not as easy as in LHD to control the detachment in the fusion reactor, where only poor measurements and actuators will be available due to the high neutron and γ-ray irradiations. Furthermore, as observed in LHD, the profile of the divertor heat load is not constant. The peak heat load will be at least a few times larger than the averaged heat load [4,7]. Although an attempt to flatten the divertor footprint distribution in the toroidal direction has been examined for FFHR-d1 by configuration optimization using additional coils [8], it is still insufficient. Therefore, in the worst case, where radiation cooling is not enough and the plasma attaches to the divertor plates, the peak heat load can exceed more than several tens of

MW/m^2 in FFHR-d1. This is not acceptable for conventional solid material divertors. Indeed, the maximum heat load of the water-cooled tungsten monoblock divertor with copper cooling pipes being developed for ITER is limited to $10 - 20$ MW/m^2 [9]. On the other hand, flowing liquid metals can tolerate high heat loads. For instance, in the International Fusion Materials Irradiation Facility (IFMIF), designs call for irradiating a liquid lithium flow with a 1 GW/m^2 deuterium beam. The liquid lithium flow in IFMIF can resist such a high heat load in steady state, since its flow velocity is as fast as $15 - 20$ m/s [10].

There are many proposed designs for utilizing liquid metals in plasma-facing components. The first proposal of liquid metal divertor was made in the design of UWMAK-1 in 1974 [11]. Application of the free surface of liquid lithium or molten salt to the first wall was also proposed in the design of the HYLIFE-I and HYLIFE-II inertial fusion reactors [12]. To keep the molten salt on the ceiling, the Kunugi-Sagara type Free surface (KSF) wall was proposed in the FFHR design, where micro grooves were made on the first wall to use the capillary force to withstand the gravitational force [13]. In the ARIES-RS design, the Convective Liquid Flow First-wall concept (CLiFF) was proposed after intensive studies of APEX [14]. The CLiFF consists of a first-wall covered with fast flowing liquid metal and a divertor with fast droplet flow. In experimental studies, lithium has been applied in many devices, since the lithium coated vacuum vessel wall is effective for hydrogen recycling reduction. For instance, the Capillary Porous System (CPS), where molten lithium oozes from a molybdenum mesh, has been successfully applied to T-11M [15], FTU [16], and TJ-2 [17]. A good energy confinement property has been demonstrated in the Lithium Tokamak eXperiment (LTX) equipped with a large area liquid lithium wall [18]. The Liquid Lithium Divertor (LLD), where the divertor is composed of porous molybdenum plates including lithium was also applied in NSTX [19]. Various ideas of flow induction have been also discussed. An application of Thermo-Electric Magneto-Hydro-Dynamics (TEMHD) was proposed as the Lithium-Metal Infused Trenches (LiMIT) [20], and tested in HT-7 as the Flowing Liquid Lithium Limiter (FLLL) [21]. In the Actively Convected Liquid Metal Divertor (ACLMD), the Lorentz force is used to drive a flow [22]. However, the simplest flow induction methods might be those that take advantage of the force of gravity. Some examples of gravity-driven systems include a jet-drop curtain of liquid gallium, which was applied as the plasma limiter in T-3M

[23], a thin liquid film formed between two knife-edge guides [24], a guide-plate type liquid metal divertor, and a free fall type liquid metal shower divertor. The latter two were already proposed in 1986 [25].

Among them, we have chosen the free fall type liquid metal shower divertor. However, a simple shower seems not suitable for our purpose. Each jet in the shower narrows after acceleration by gravity. And what is worse, a jet easily transforms to droplets due to the surface tension instability [26]. Use of wires, tapes, or chains as an Internal Flow Resistance (IFR) is effective to stabilize the jet. When a jet is falling along an IFR, the jet flow velocity finally reaches the terminal velocity, because the friction force balances the gravitational force. The basic idea of REVOLVER-D is to use the liquid metal shower jets stabilized by IFRs.

This paper describes the conceptual design of REVOLVER-D in FFHR-d1. The overall picture together with the details of the jets stabilized by IFRs and the limiter/divertor concept are described in the next section. Numerical evaluations of the permissible heat load, the liquid metal pump power, and the vacuum pressure are given in Section 3. The magnetic field environment surrounding the REVOLVER-D is discussed in Section 4. Finally, these discussions are summarized in Section 5.

2. The overall picture of REVOLVER-D

A bird's eye view of the FFHR-d1 equipped with the REVOLVER-D is shown in Fig. 1. The REVOLVER-D is composed of ten similar units. One unit consists of a liquid metal pump, ducts, an upper unit (shower head with IFRs), a lower unit (pool), and a heat exchanger. Maintenance of the liquid metal pump, the upper unit, and the cooling panels in the heat exchanger is easy since these can be removed by simply pulling them up. It is also possible to use the large outer and/or upper ports, if the breeding blankets are already removed for maintenance. In the device center, a central vacuum vessel is installed and connected to the main vacuum vessel via ten inner ports equipped with maze neutron shields. This central vacuum vessel is designed to enhance the vacuum pump efficiency by minimizing the conductance between the main vacuum vessel and the vacuum pumps consisting of cryopanel units and Turbo Molecular Pumps (TMPs). The maze neutron shield protects the components in the central vacuum vessel from direct irradiation by 14 MeV neutrons, while keeping a

4

high conductance for efficient vacuum pumping. Although a detailed design work should be done in future, it will basically have a maze structure as seen in Fig. 1. The cryopanel units, TMPs, liquid metal pumps, and High-Temperature Superconductor Central Solenoids (HTS-CS) are installed inside the central vacuum vessel. The main purpose of the HTS-CS is to shield the pumps from the strong magnetic field. A strong vertical magnetic field of 5 T exists in the central region of FFHR-d1 (with the present magnetic configuration), where liquid metal pumps and TMPs are installed. This magnetic field can be shielded by using the HTS-CS. The magnetic field distribution with or without HTS-CS will be discussed in Section 4. The cryostat for the HTS-CS is set inside the central vacuum vessel as shown in Fig. 1. There is a large space inside the cryostat for the HTS-CS and it is possible to install additional neutron shields to protect the SC coils from the streaming neutrons, if necessary. Detailed design studies on the HTS-CS, cryostat, supporting structure, neutron shield, together with the neutronics simulation are remained for future study.

In the heliotron configuration as in LHD and FFHR-d1, the so-called ergodic layer surrounds the Last-Closed-Flux-Surface (LCFS). A magnetic line of force started from just outside the LCFS travels inside the ergodic layer for more than several hundreds of meters even in LHD [4], which is four times smaller than the FFHR-d1. Therefore, if the liquid metal shower is set inside the ergodic layer as in Fig. 2, a significant portion of magnetic lines of force finally hit the showers. Then, the plasma heading for the divertor region along the magnetic lines of force also hits the shower and disappears. From this point of view, the liquid metal shower of REVOLVER-D plays a role of a limiter inserted to the ergodic layer. A similar idea has been already proposed as the Helical X-point Divertor (HXD) [27], where solid target plates are placed near two X-points helically rotating along the torus. In the HXD, the heat load on the target plates is reduced by expanding the plasma-wetted area as large as possible. However, this makes the maintenance difficult at the same time. The plasma-wetted area is quite small and the heat load is significantly larger in the REVOLVER-D. Nevertheless, these operating conditions are acceptable because flowing liquid metal is used, as will be discussed in Section 3.1.

Figure 3 shows an example of nozzle layout, where 28 nozzle units drawn by large circles are arranged in five rows that are each separated by one degree in the toroidal direction. Each of the

nozzle units has two nozzles with a diameter of 20 mm or 40 mm drawn by small circles and 56 liquid metal jets in total are issued from these nozzles. The jets should be arranged to interfere as much as possible with the magnetic lines of force. From this point of view, there still is room for optimization in the nozzle layout shown in Fig. 3. The majority of the heat load is absorbed inside the shower and this is why we call this the "effectively volumetric divertor." On the other hand, at least one-half of the neutral particles generated inside the shower go to the vacuum pump side (downward direction in Fig. 3(b)), since the conductance in this direction is larger than those of the other directions. Essentially, the shower is transparent for neutrals while it is a rigid wall for plasmas. Therefore, the REVOLVER-D is not only the ergodic limiter but also the divertor, *i.e.*, the ergodic limiter/divertor, with a high pumping efficiency. Details of the vacuum-pumping scenario in REVOLVER-D will be discussed in Section 3.3.

The falling length of the jets is as long as ~4 m in the REVOLVER-D for FFHR-d1. In the case of a free jet, it is accelerated by gravity and easily transforms to droplets. It is difficult to stop the plasma heading for the vacuum vessel wall by the discrete droplets. In the REVOLVER-D, as explained in the introduction, an IFR is inserted to each jet. A jet falling along an IFR scarcely transforms to droplets. In Fig. 4, examples of water jet without or with IFR are shown. Droplet formation in the case of free jet as seen in Fig. 4(a) can be easily prevented by inserting a metal chain to the jet (Fig. 4(b)). The IFR should be carefully chosen by taking into account the geometry and velocity of the jet. In Figs 4(c)-(f), shown are the cases of bold and fast jets without or with wire/tape/chain. Among these four cases, the tape seems to be the best IFR since the jet surface is relatively stable. The chain that works well in the case of narrow and slow water jet (Fig. 4(b)) is apparently not applicable to a bold and fast water jet since it largely scatters the jet as seen in Fig. 4(f). In Figs. 4(g) and 4(h), compared are the bold and fast water jets issued from a slanted nozzle without or with a tape as IFR. In this case, the tape shows a proper flexibility and follows the water jet. At the same condition, both wire and chain did not follow the jet and became exposed (not shown). Note that these are the results obtained in the case of water jet. The optimum IFR for the liquid metal jet can be different from that for the water jet. The optimum IFR should stabilize the jet surface, and at the same time, it should properly drive turbulence inside the jet to mix the different temperature regions (see

6

discussions in Section 3.1) and follows the jet even if the jet is curved (see discussions in Section 4.2). The material of IFR will be chosen from ceramics, since it should be nonmagnetic and, if possible, light, strong, electrically insulating, and resistant to corrosion.

Pure molten tin (Sn) is the first candidate of the liquid metal for REVOLVER-D, because of its low melting temperature (~505 K) and low vapor pressure (< 10^{-5} Pa at < 1,000 K [28]). Alloys, *e.g.*, lithium-tin [29,30], are not selected as the first candidate for the REVOLVER-D to avoid difficulties related to the composition management in the fusion reactor environment. Characteristics of low melting point metals of lithium (Li), sodium (Na), gallium (Ga), indium (In), tin, lead (Pb), and bismuth (Bi), are compared in Table 1, where numerical values are taken from Refs. 28 and 31. Among these metals, tin has the lowest vapor pressure. Figure 5 compares the vapor pressure of the metals listed in Table 1. Thick solid lines in Fig. 5 for Li, Pb, and Sn are calculated by using equations given in [28]. For example, the vapor pressure of molten tin, p_{Sn} (Pa), is given by

$$p_{Sn} = 65.42 \times 10^9 \exp\left(-\frac{37,190}{T}\right), \tag{1}$$

where T is the temperature in K. The vapor pressure of Na is roughly 100 times larger than that of Li compared at ~1,000 K. The vapor pressures of Ga and In are roughly 10 times larger than that of Sn compared at 1,500 – 2,000 K.

The specific heat of tin, C_{Sn}, is 253 J/(kg·K) at 510 K and linearly decreases to 230 J/(kg·K) at 800 K [32]. The viscosity coefficient of tin is similar to that of water. Since the density of tin is roughly seven times larger than water, the kinematic viscosity coefficient of tin is ~1/7 times that of water. The surface tension of tin is in the range of 440 – 540 mN/m at 500 – 1,050 K [33]. This is roughly seven times larger than that of water (~73 mN/m) and similar to that of mercury (~475 mN/m) at 293 K. These differences between tin and water should be carefully taken into account in the simulation experiment using water as in Fig. 4. Tin is easily oxidized especially near the melting point. Tin has a strong corrosivity. Corrosion of solder pots is one of the issues in lead-free soldering, where the component ratio of tin is high. It has been reported that corrosion of stainless steels by tin can be

mitigated by forming a chromium oxide layer at 1,200 °C [34]. The wettability of tin with ceramics is quite low, *e.g.*, the wetting angle on the alumina (Al_2O_3) plate is 160 – 175 degrees at 500 – 1,050 K [33]. The reactivity of tin with ceramics is also quite low [30]. Therefore, it is recommended to use ceramic pipes reinforced by metal pipes (or, metal pipes with thick ceramic coating inside, at least) for the ducts. In any case, as will be discussed below, one should use ceramic insulating pipes to avoid large MHD pressure loss in the liquid metal system of magnetic confinement fusion reactors.

Low material cost, low toxicity, no explosive reaction with water, and high nuclear stability are also the merits of tin. Indeed, tin has been utilized safely and widely in the world, as the main component of solder, or "tin cans," *etc*. The atomic number of tin is 50, which is one of the magic numbers. It is well known that an atomic nucleus containing the magic number is relatively stable against nuclear decay and has many stable isotopes. Tin has 10 stable isotopes. On the other hand, tin has 28 unstable isotopes. It should be noted that ^{113}Sn, ^{117m1}Sn, ^{119m1}Sn, ^{121m1}Sn, ^{123}Sn, ^{125}Sn, and ^{126}Sn have relatively long half-lives of 115 days, 14 days, 293 days, 55 years, 129 days, 10 days, and 2.4 $\times$ 10^5 years, respectively. According to the analysis by EASY-2005 [35], ^{125}Sb, which is generated from ^{125}Sn, will be the dominant radioactive isotope at ~10 years after shutdown. The main radioactive wastes emitted from the REVOLVER-D will be oxidized tin and chains. The total amount of the circulating tin is ~360 tons (~51 m^3). Since tin is a high Z material near Xe, the sputtered tin can be an efficient radiator for divertor heat load reduction. The vapor shielding effect of tin reported in [36] will also be helpful. This effect is especially important in a system using the static molten tin surface formed on the CPS as proposed in [37]. On the other hand, contamination of the main plasma by tin should be prevented. In the case of REVOLVER-D, the impurity shielding effect of the ergodic layer as observed in LHD [38-40] will be beneficial. Especially in Ref. 38, effective screening of iron impurities originated from the metallic vacuum vessel wall by the ergodic layer is discussed. It was observed that the influx of iron ions to the core plasma normalized by the source term decreased with the density. This means that the friction force, which pushes the impurity ions out from the ergodic layer, dominates the iron impurity transport in the ergodic layer, since the friction force increases with the density. It is also discussed in Ref. 38 that the friction force enhances for the heavier ions leading to an efficient impurity screening. This gives a hopeful qualitative prediction that the contamination of

the core plasma by tin can be suppressed in the reactor condition with a higher density than in LHD. Nevertheless, the transport of tin should be clarified quantitatively by both numerical simulation and experimental studies in the future.

3. Numerical evaluations

3.1. Tolerable heat load

The fusion output in FFHR-d1 is ~3 GW and 1/5 of this (= 600 MW) is the alpha heating power that should be removed by the first wall and divertor. In high-density attached plasmas in LHD, ~30 % radiation loss is usually observed [6]. Light impurities, *e.g.*, carbon and oxygen, are considered to be the main radiators in LHD. In the discussions below, we assume a moderate radiation loss of 30 % as in LHD, since the quantitative evaluation of radiation loss in FFHR-d1 equipped with REVOLVER-D, where tin will be one of the main impurities, is not yet performed and remains for the future work. The plasma-wetted area in the limiter/divertor configuration of REVOLVER-D depends on the accurate positioning of the molten tin shower. Its quantitative evaluation also remains for the future work. Here, we assume a plasma-wetted area of 0.125 m^2 (~ (1/2) × 1 m × 0.25 m, see Fig. 15 in Section 4.2). Since the shower is set at each of the 10 inner ports in FFHR-d1, the heat flux on one side of a shower, Q_{heat}, is estimated to be Q_{heat} = 600 MW × 70 % / 10 / 2 / 0.125 m^2 = 168 MW/m^2. The temperature increase from the initial temperature of T_0 to $T_1 = T_0 + \Delta T$ is given by

$$\Delta T = \frac{Q_{heat}S}{Q_{mass}\,C_{Sn}} \,, \tag{2}$$

where S, Q_{mass}, and C_{Sn} are the projected area of the heat flux on the jet, the mass flow rate, and the specific heat of tin, respectively. In Fig. 6, T_1, ΔT, and p_{Sn} at T_1 calculated by Eqs. (1) and (2) for a molten tin jet of 40 mm diameter and T_0 = 523 K heated by Q_{heat} = 168 MW/m^2 on S = 0.04 m × 1 m, are plotted with respect to the flow velocity. Here, we used a constant C_{Sn} of 220 J/(kg·K). As seen in Fig. 6, the vapor pressure of tin can be kept at ≤ 0.0024 Pa (T_1 ≤ 1,200 K), as long as the jet flow velocity is ≥ 5 m/s. This vapor pressure is low enough compared with the exhaust pressures of

hydrogen isotopes and helium of ~1.3 Pa and ~0.05 Pa, respectively, as will be evaluated in Section 3.3.

These estimations are valid only if the turbulence inside the jet is large enough to mix up the high and low temperature regions. If this is not the case and the flow is laminar, the surface temperature on the heated side of the jet becomes much higher than the estimation above. In Figs. 7 and 8, shown are the simulation results given by the finite element method code ANSYS, for the case of laminar jet without IFR. In the simulation, a liquid tin jet of 40 mm diameter vertically falling for 2 m at a constant velocity of 5 m/s is assumed. The heat load of 168 MW/m^2 is applied on the jet from one side with a cosine profile for 1 m of the vertical length. A constant C_{Sn} of 220 J/(kg·K) is also used here. The flow is assumed to be laminar and therefore there appears a strong temperature gradient from front to back sides with respect to the heat load. Profiles in the vertical (z) direction of the local temperature at the front side, T_{front}, that on the jet center, T_{center}, and that at the back side, T_{back}, together with the temperature averaged over the jet cross-section at z, T_{ave}, are shown in Fig. 8. Note that the T_{ave} is identical to the T_1 discussed in the former paragraph and shown in Fig. 6. The peak of T_{front} reaches 2,400 K in this laminar jet case. Needless to say, this is not acceptable, since the vapor pressure exceeds 10^4 Pa at this temperature (see Fig. 5). It is inevitable to drive turbulence inside the jet and mix up the temperature profile to decrease T_{front} and T_{center} to the level of T_{ave}. Therefore, the role of IFR to enhance the turbulence inside the jet while keeping the jet surface stable is quite important. The IFR should also have proper flexibility at the same time, as will be discussed later (Section 4.2). For example, a ceramic fiber tape with bumps and dents is a strong candidate of the IFR that can satisfy these requirements.

It should be noted that the temperatures discussed above was the maximum value. The maximum temperature will be reached at a limited area of each jet. Therefore, the IFRs in such jets should be tolerant with the high-temperature exceeding 1,200 K. In the pool that receives the shower jets, however, these high-temperature jets become mixed with the low-temperature jets that suffer no or low heat loads. One unit of the REVOLVER-D is equipped with 56 jets, of which 44 jets have 20 mm diameter and the other 12 have 40 mm diameter (see Fig. 3). At a flow velocity of 5 m/s, the mass flow rates of molten tin jets of 20 mm and 40 mm diameter are ~11 kg/s and ~44 kg/s, respectively.

Note that we here use an identical flow velocity for the two nozzles with different diameters, for simplicity. As long as the inlet pressure and nozzle length are fixed, the flow velocity decreases with the nozzle diameter, since the pressure loss is inversely proportional to the nozzle diameter and proportional to the nozzle length. In other words, it is possible to control the outlet velocity by adjusting the inlet pressure and/or nozzle length. The total mass flow rate of 560 jets in 10 inner ports is then given by $(11 \times 440 + 44 \times 120) \sim 10$ ton/s $\sim 36,000$ ton/h. The averaged temperature increase of 560 jets, ΔT_{ave}, heated by 600 MW $\times$ 70 % = 420 MW is calculated to be $\Delta T_{ave} = 420$ MW / $(10^4$ kg/s) / (220 J/(kg·K)) ~ 190 K. The averaged temperature becomes ~ 710 K, if the initial temperature is 523 K. This is low enough to enable use of typical Reduced Activation Ferritic/Martensitic (RAFM) steels, of which the maximum available temperature limit will be around 800 K [41]. At the same time, it will be possible to generate electricity from the divertor exhaust heat with $\Delta T_{ave} \sim 190$ K. Details of the heat exchanger (see Fig. 1) are not determined yet.

3.2. Liquid metal pump power

As was discussed in the previous section, the total mass flow rate of molten tin in the REVOLVER-D is $\sim 36,000$ ton/h. To circulate this mass flow, 10 pumps of 3,600 ton/h are expected to be used. It will be possible to realize this mass flow, even though new R&D studies are needed, since three sodium pumps of 5,100 ton/h (15,300 ton/h in total) was already operated in the Japanese fast breeder reactor "Monju" [42]. Figure 9 shows the schematic view of the molten tin flow channel in one of the 10 sections in the REVOLVER-D. The molten tin flows from A to N in alphabetical order. Double pipes, in which outer metal pipes reinforce inner ceramic pipes, are necessary to transfer the molten tin across the strong magnetic field. Main parameters of the molten tin flow channel are summarized in Fig. 10. This figure is obtained by assuming a flow velocity at the shower of 5 m/s and a constant mass flow rate of $\sim 3,600$ ton/h along the channel. The pressure loss and pump power under this condition have been evaluated [43]. In Ref. 43, the flow velocity of the shower jets was assumed to be ~ 3.7 m/s, while other conditions, *e.g.*, the flow path, the inner diameter and the length of ducts, *etc.*, were identical to those shown in Fig. 10. Therefore, we have reevaluated the case with 5 m/s of the shower

jet velocity using the same procedure used in [43]. In the case of $v = 5$ m/s, the total pressure loss is ~0.85 MPa, in which the MHD loss is ~0.17 MPa, and the total pump power needed to circulate molten tin at all 10 sections is ~14.4 MW. If we assume conducting pipes, the total pressure loss increases to ~34 MPa and the pump power also increases to ~430 MW. Therefore, use of insulated pipes is inevitable.

3.3. Vacuum pressure

Regarding the neutral particle exhaust, an ~~enough~~ sufficient pumping speed, which is high enough to maintain the divertor pressure as low as that observed in present experiments, is required for the REVOLVER-D as the divertor. The neutral exhaust gasses mainly composed of hydrogen isotopes of deuterium (D) and tritium (T), *i.e.*, D_2, DT, and T_2, and helium (He) ash generated by DT fusion reaction, together with a small amount of H_2, HD, HT, are exhausted along the path shown in Fig. 11. These exhaust gasses generated in the shower are led to the central vacuum vessel via a maze neutron shield (A in Fig. 11). A part of the exhaust gasses rises to the cryopump region surrounded by the 80 K thermal shield via gaps of the HTS-CS of ~1 m height (B in Fig. 11). The cryopanel unit inside the 80 K thermal shield finally absorbs the hydrogen isotopes. Another part of the gasses including helium goes down via gaps of the HTS-CS (C in Fig. 11) and is exhausted by the TMPs. A close-up view of the 80 K thermal shield and cryopanel units is shown in Fig. 12.

First, let us consider the vacuum pumping by the cryopump. Conductances of C_A and C_B at A and B in Fig. 11 are evaluated by using the formula below [44]:

$$C_{\text{rectangular}} = \frac{300na^2b^2\sqrt{T/293}}{(a + b)L\sqrt{M/29}} \,, \tag{3}$$

where $C_{\text{rectangular}}$ (m^3/s), n, a (m), b (m), L (m), T (K), and M are the conductance of a rectangular tube, the number of similar components connected in parallel, the tube width, the tube height, the tube length, the gas temperature, and the molecular weight of the exhaust gas. Then, we obtain $C_A \sim 930$ m^3/s and $C_B \sim 600$ m^3/s, using (n, a, b, L, T, M) = (10, 1.6 m, 0.86 m, 6.0 m, 293 K, 5) and (10, 1.0 m,

0.7 m, 1.8 m, 80 K, 5) for C_A and C_B, respectively. The total conductance of C_A and C_B connected in series then becomes ~365 m^3/s. The hydrogen isotope gasses are absorbed (or, condensed) to one of ten cryopanel units installed in the cryopump. The reason why only one unit is used at once will be explained below. The total surface area of one cryopanel unit is ~20 m^2. The pumping speed of a cryopump is basically determined by the conductance of the vacuum-pumping path including the pump inlet, since the condensation probability of hydrogen isotopes to the cryopanels can be assumed to be ~1. Here, we assume a conservative effective pumping speed including the path conductance to be 300 m^3/s, instead of 365 m^3/s. This is not an extremely large value even compared with the effective pumping speed in ITER of 200 m^3/s [45].

To pump out the helium ash generated by the DT fusion reaction, 26 TMPs are installed in the bottom of the central vacuum vessel. Here, we assume the pumping speed per a TMP of 5 m^3/s for both hydrogen isotopes and helium gasses. This is the value available to date. Eleven TMPs are directly connected to the bottom flange of the central vacuum vessel and other 15 TMPs are connected via circular pipes of 0.3 m diameter and 0.7 m length, as shown in Fig. 13. The effective pumping speed of these TMPs is evaluated by using a formula of conductance of a cylindrical tube [44], *i.e.*,

$$C_{\text{cylinder}} = \frac{121 K d^3 \sqrt{T/293}}{L\sqrt{M/29}} ,$$

(4)

where C_{cylinder} (m^3/s), K, and d (m) are the conductance of a circular tube, a correction factor for short pipes, and the tube diameter, respectively. The conductance of each tube is calculated to be 4.0 m^3/s, using (K, d, L, T, M) = (0.36, 0.3 m, 0.7 m, 293 K, 5). The effective pumping speed of the 26 TMPs as a whole is then becomes 11 × 5 + 15 × (1/4 + 1/5)$^{-1}$ ~ 90 m^3/s. Here, we apply this value for both hydrogen isotopes and helium gasses for simplicity.

In a fusion reactor of 3 GW fusion output, the DT fusion reaction takes place 3 × 10^9 / ((3.52 + 14.06) × 10^6 × 1.6 × 10^{-19}) ~ 1.07 × 10^{21} times per second. Hereinafter, we assume the D/T ratio to be 50/50 and the "burnup fraction," which is defined as the number ratio of burned DT particles to the fueled DT particles, to be 1 %. In this case, 1.07 × 10^{21} of helium atoms are generated from 2.14 × 10^{23}

of D and T atoms per second. At a room temperature of 25 °C, these correspond to the He generation rate of ~4.4 Pa·m^3/s and the DT fueling rate of ~440 Pa·m^3/s, respectively. However, the DT fueling rate has a large ambiguity since it depends on the burnup fraction. In the discussions below, we will use the DT fueling rate of 500 Pa·m^3/s, which roughly corresponds to 1 g/s, for simplicity. In a fusion reactor, all of the supplied DT fuel and generated He ash should be exhausted in steady state. Since the effective pumping speed of the cryopump and TMPs for DT is 300 + 90 = 390 m^3/s and that for He by TMPs alone is 90 m^3/s, the exhaust pressures of DT and He are evaluated to be ~1.3 Pa and ~0.05 Pa, respectively. These are similar to those observed in the present experiments.

Tritium inventory is one of the most important issues in using cryopumps in a fusion reactor. From the perspective of safety, strict limitation will be imposed on the tritium inventory in the reactor. In ITER, for example, the tritium inventory inside the vacuum vessel is limited to 1 kg, and 120 g of this is attributed to the cryopump [46]. As discussed above, the DT fuel will be supplied at 1 g/s in FFHR-d1. Therefore, the T atoms have to be exhausted by the cryopump at a rate of 0.6 g/s. This means that the cryopanel unit retains 600 g of T atoms after 1,000 seconds operation. This is 5 times larger than that expected in ITER. However, this will be permissible since the first-wall temperature in FFHR-d1 is expected be > 500 °C, which is much higher than that in ITER of < 200 °C, and therefore the tritium inventory of the first-wall in FFHR-d1 will be much smaller than that expected in ITER. In the REVOLVER-D, ten cryopanel units are prepared. These are normally placed inside metal tubes. In operation, one of the ten units is pulled down from the metal tube by using the bellows unit (see Fig. 1) and exposed to the exhaust gasses. After 1,000 seconds exposure, this unit is pulled up into the metal tube and the next unit is pulled down, and so forth. The used cryopanel unit retaining 600 g of T is heated inside the metal tube for hydrogen isotope desorption. It is also possible to introduce a warm He gas, or another gas, into the metal tube to accelerate the temperature increase. After completion of hydrogen desorption, this unit is cooled down again. This process of temperature-programmed desorption and re-cooling should be completed while the other nine units are working one by one, *i.e.*, 9,000 seconds = 2 hours and 30 minutes in our case. If this process can be completed within 30 minutes, one can shorten the exposure time to 200 seconds and reduce the tritium retention to 120 g.

As for the exhaust capacity, 500 Pa·m^3/s × 1,000 sec = 500,000 Pa·m^3 is required for one cryopanel unit. This will be feasible, since the cryopump developed for the LHD closed divertor system has already demonstrated ~13,600 Pa·m^3 of the exhaust capacity by using three cryopanel units of which the total surface area is ~0.57 m^2 [47]. Therefore, ~500,000 Pa·m^3 of the exhaust capacity can be achieved by a cryopanel unit with ~20 m^2 of the total surface area.

4. Magnetic field environment

4.1. Radial field

For whomever wants to use liquid metals in a magnetic confinement fusion reactor, the most important issue is the magnetic field. Distributions of the magnetic field in FFHR-d1 are depicted in Fig. 14. The radial magnetic field, B_r, shown in Fig. 14(a), is as large as ~3 T near the inner poloidal coils. However, this magnetic field component is parallel to the flow direction and therefore is not considered to be critical. Strictly speaking, this field can induce a circumferential electric current perpendicular to the liquid metal flow. The Lorentz force due to this current and the toroidal magnetic field, B_t, or the vertical magnetic field, B_z, may affect the flow pattern of the liquid metal.

4.2. Toroidal field

The B_t is quite small along the liquid metal channel, as is shown in Fig. 14(b). However, the B_t becomes as large as ~1.5 T at where the liquid metal jet touches the plasma in the ergodic layer. The Lorentz force induced by the B_t and the electric current flowing from the plasma into the jet can bend the jet significantly. Since the electric resistivity of tin is quite small (~10^{-7} Ω·m), a small voltage can induce a large electric current. In the REVOLVER-D, molten tin jets are inserted into the ergodic layer. Since the electric potential is not constant inside the ergodic layer, a large electric current can be induced in the jets. The maximum electric current may be given by the ion saturation current, I_{sat}. The equation below gives an ion saturation current per a unit area, I_{sat}/S (kA/m^2), *i.e.*,

$$\frac{I_{\text{sat}}}{S} = n_e e \sqrt{e} \sqrt{\frac{1}{m_i} \frac{kT_e}{e}} \exp\left(-\frac{1}{2}\right), \tag{5}$$

where n_e (m^{-3}), m_i (kg), and kT_e/e (eV) are the electron density, the ion mass, and the electron temperature, respectively. In the case of the DT plasma with the atomic weight of 2.5, this equation can be simplified as below:

$$\frac{I_{\text{sat}}}{S}(\text{kA/m}^2) \sim 6.0\, n_e(10^{19}\,\text{m}^{-3})\sqrt{T_e(\text{eV})}\ . \tag{6}$$

In Section 3.1, we have evaluated the maximum heat flux on the liquid metal shower to be 168 MW/m^2. If we assume, for example, n_e and T_e of 4×10^{19} m^{-3} and 100 eV, respectively, then we obtain $I_{\text{sat}}/S \sim 240$ kA/m^2 and the divertor heat load of P_{div} (MW/m^2) = 7 × I_{sat}/S (kA/m^2) × T_e (eV) /1,000 = 168 MW/m^2. However, it is unlikely that this maximum ion saturation current is flowing into a jet at the entire jet surface inside the ergodic layer, because both n_e and T_e are not constant in the ergodic layer. The net current from the plasma to the outside of vacuum vessel through the jet should be zero to keep the ambipolarity. What we should consider is the local current along the jet intersecting two positions with different electric potential, since both n_e and T_e (and therefore the electric potential) can vary inside the ergodic layer.

Here, let us consider a model case where the maximum ion saturation current of 240 kA/m^2 is flowing into a jet at $z = \pm0.05$ m and returns to the plasma at $z = \pm0.5$ m, as depicted in Fig. 15. The maximum ion saturation current into a jet of 0.04 m diameter is 960 A. The half of this, *i.e.*, $I = 480$ A, is flowing up the jet and another half is flowing down the jet. In this situation, the Lorentz force, F, working on an element of molten tin of $d = 0.04$ m and $L = 0.04$ m ($m \sim 0.35$ kg), falling at a constant vertical velocity of $v = 5.0$ m/s in a toroidal magnetic field of $B = 1.5$ T, is given by $F = ILB = 28.8$ N in the radial direction. At $z = +0.5$ m to 0 m, the electric current is flowing upward. The time, t, needed for the molten tin element to pass through this region is given by $t = 0.5 / 5.0 = 0.1$ s. Then, the radial displacement of the element after falling from $z = 0.5$ m to 0 m is evaluated to be $(1/2)\,(F/m)\,t^2 \sim 0.41$

m. Just below this, *i.e.*, at *z* = 0 m to -0.5 m, the electric current flows downward and the Lorentz force works in the opposite direction. Finally, the element returns to the original radial position. This situation is schematically drawn in Fig. 16. One should carefully determine the toroidal field direction to set the bending direction of the jet toward the torus center, not to the core plasma.

However, we need further consideration since the radial displacement of 0.41 m is quite large. As can be seen in Fig. 15, the jet deviates from the plasma boundary determined by the limiter/divertor denoted by a broken curve in Fig. 15, if it radially bends more than ~0.25 m. Outside of the plasma boundary, no electric current flows into the jet and the Lorentz force disappears. Therefore, the maximum radial displacement of the jet nearest to the core plasma can be considered to be ~0.25 m. The same situation occurs when the jet aligns with the equipotential surface in the ergodic layer. If this takes place, the radial displacement of the jet can be smaller. It will decrease further as the radiation cooling of the plasma in the ergodic region by tin ions becomes enhanced. Since the ion saturation current is proportional to the density and the square root of the temperature (see Eqs. (5) and (6)), plasma cooling by inserting the liquid metal shower into the ergodic layer as a limiter and enhancing the radiation loss by tin is effective in mitigating the Lorentz force. The vapor shielding effect [36] is also favorable for this. If these work properly without contaminating the core plasma, then the radial displacement of the jet becomes zero and the jet straightly falls down to the pool.

In conclusion, a jet in the ergodic layer will bend and finally align with the plasma boundary at worst. Even in the worst case, there is no critical problem ~~as long as~~ if only the IFRs inside jets are not exposed to the plasma. This is one of the important issue remained for the future study. As is ordinarily experienced, a long but light object in a fluid follows the fluid motion as was shown in Fig. 4(h). Establishment of a numerical model and validation of it by experiment is needed in order to know how to prevent exposure of the IFR to the plasma. Again, a ceramic fiber tape with bumps and dents suggested in Section 3.1 can be a strong candidate for the IFR. The radial displacement of the jet will decrease the heat load projection area on each shower and increase the temperature of some jets. Then, the vapor pressure of tin increases. However, the increased tin vapor pressure may enhance the radiation cooling and the radial displacement of the jet decreases as a result. The key issue for this scenario is the impurity shielding effect of the ergodic layer. This should be clarified as soon as

possible in the future study. In the discussions above, it was assumed that the exit end of the IFR is not under any tension at all, and therefore the IFR can deform along the jet. What will happen if the IFR is fixed to the pool with proper tension? Two extreme examples can be imagined for this, *i.e.*, the jet bends due to the Lorentz force and the IFR is left, or the surface tension will constrain the flowing tin to the IFR despite the Lorentz force. In the former case, the jet will break up into droplets and the IFR will be hit by hot plasmas, while the latter case is preferable. This point should be also discussed in the future study.

4.3. Vertical field

As shown in Fig. 14(c), a strong B_z of ~5 T exists in the central region of FFHR-d1, where liquid metal pumps and TMPs will be installed. A magnetic shield is inevitable for using these pumps. Since there is no material that can shield 5 T (*e.g.*, the saturation magnetic flux density of Permendur, a cobalt-iron soft magnetic alloy, is ~2.3 T), we consider using HTS-CS coils for the magnetic shield. The HTS-CS coils are enclosed by cryostats and placed inside the central vacuum vessel (see Fig. 1). Using this HTS-CS, the B_z in the central region can be reduced to < 0.5 T, as is shown in Fig. 14(d). Then, it becomes possible to completely shield the magnetic field by using normal magnetic shield materials. The vertical field generated by the HTS-CS slightly moves the magnetic axis outward. In the case of Fig. 14(d), the magnetic axis moves from 14.4 m to 14.5 m, which corresponds to 3.60 m to 3.63 m in LHD. This outward shift can be easily compensated for by canceling the vertical field of HTS-CS using the poloidal field coils of FFHR-d1.

6. Summary

A new liquid metal divertor system named the REVOLVER-D has been proposed for the helical fusion reactor FFHR-d1. The REVOLVER-D is a limiter/divertor consisting of 10 sets of molten tin shower jets inserted to the inner ergodic layer of horizontally elongated magnetic surfaces. The molten tin jets are stabilized by ceramic IFRs of wires/tapes/chains. The total mass flow of 560 molten tin jets of 20 mm or 40 mm diameter and 5 m/s flow velocity is ~36,000 ton/h. The maximum temperature of the molten tin jet will be ~1,200 K at the maximum heat load of ~170 MW/m^2 inside the ergodic layer.

Nevertheless, the vapor pressure of tin is kept as low as ~0.0024 Pa. The averaged temperature increase of the molten tin in the pool is ~190 K. Therefore, ordinary RAFM steels can be used as the structure material of REVOLVER-D. The total pressure loss of molten tin is ~0.85 MPa including ~0.17 MPa of the MHD pressure loss, and the total pump power needed to circulate molten tin is ~14.4 MW, as long as insulated pipes are used. The neutral gas generated from the plasma hitting the molten tin shower is exhausted by the cryopump and TMPs. The exhaust pressures of hydrogen isotopes and helium are evaluated to be ~1.3 Pa and ~0.05 Pa, respectively. The tritium inventory in the cryopump is 600 g at the maximum. The Lorentz force induced by the toroidal magnetic field and ion saturation current will significantly bend a jet until it aligns to the plasma boundary or the equipotential surface. This is not critical for the REVOLVER-D, if only the IFR inside the jet is not exposed to the plasma. Therefore, it is especially important to give quantitative conditions to keep the IFR inside the bending jet. The liquid metal pumps and TMPs can be installed on the central region of FFHR-d1 by applying the HTS-CS as the magnetic shield.

As was mentioned in the Introduction, the divertor in a fusion reactor should satisfy at least five requirements of high heat load tolerance, high maintainability, ~~enough~~ sufficient vacuum pump speed, high level of safety, and a small amount of radioactive wastes. The REVOLVER-D has a good possibility to satisfy these at the same time. However, many unsolved issues still remain. To solve these, we are planning four steps of R&D in parallel with simulation studies, *i.e.*, 1) heat load test of a molten tin jet, 2) examination of the MHD effect and clarification of the conditions to prevent exposure of IFRs, together with development of efficient insulating pipes to reduce the MHD drag force, 3) plasma irradiation test to investigate the sputtering and hydrogen retention of molten tin, and, finally, 4) comprehensive demonstration in a reactor-relevant environment as, for example, in LHD. Study on the impurity shielding effect of the ergodic layer in the reactor condition is also quite important for the physics scenario of the REVOLVER-D. Particle transport simulation on the hydrogen isotopes, helium ions, and impurity ions including tin, in the ergodic layer limited by liquid tin shower jets should be performed before the comprehensive demonstration.

Acknowledgments

References

[1] A. Sagara, et al., Fusion Eng. Des. 89 (2014) 2114.

[2] J. Miyazawa, et al., Nucl. Fusion 54 (2014) 043010.

[3] A. Komori, et al., Fusion Sci. Tech. 58 (2010) 1.

[4] S. Masuzaki, et al., Nucl. Fusion 42 (2002) 750.

[5] J. Miyazawa, et al., Nucl. Fusion 44 (2004) 154.

[6] J. Miyazawa, et al., Fusion Sci. Tech. 58 (2010) 200.

[7] M. Shoji, et al., Fusion Sci. Tech. 58 (2010) 208.

[8] N. Yanagi, et al., Proc. of the 24th IAEA Fusion Energy Conf. (San Diego, USA, October 2012) FTP/P7-37.

[9] J. Schlosser, et al., Nucl. Fusion 45 (2004) 512.

[10] M. Ida, et al., Fusion Eng. Des. 63-64 (2002) 333.

[11] B. Badger, et al., 'UWMAK-I - A Wisconsin Toroidal Fusion Reactor Design' UWFDM-68 (1974).

http://fti.neep.wisc.edu/pdf/fdm68.pdf

[12] R.W. Moir, Particle Accelerators 37-38 (1992) 467.

[13] A. Sagara, et al., Fusion Sci. Tech. 47 (2005) 524.

[14] M.A. Abdou, et al., Fusion Eng. Des. 54 (2001) 181.

[15] S. Mirnov, J. Nucl. Mater. 390-391 (2009) 876.

[16] G Mazzitelli, M.L. Apicella, A. Alexeyev, FTU Team, Fusion Eng. Des. 86 (2011) 580.

[17] F.L. Tabarés, et al., J. Nucl. Mater. 463 (2015) 1142.

[18] J.C. Schmitt, et al., Phys. Plasmas 22 (2015) 056112.

[19] H.W. Kugel, et al., Fusion Eng. Des. 87 (2012) 1724.

[20] D.N. Ruzic, W. Xu, D. Andruczyk, and M.A. Jaworski, Nucl. Fusion 51 (2011) 102002.

[21] G.Z. Zuo, et al., Fusion Eng. Des. 89 (2014) 2845.

[22] M. Shimada and Y. Hirooka, Nucl. Fusion 54 (2014) 122002.

[23] S.V. Mirnov and V.A. Evtikhin, Fusion Eng. Des. 81 (2006) 113.

[24] F. Okino, R. Kasada, S. Konishi, Fusion Eng. Des. 89 (2014) 1054.

[25] K. Maki, 'Tokamak Concept Innovations' IAEA-TECDOC-373 (1986) 87.

http://www.iaea.org/inis/collection/NCLCollectionStore/_Public/17/056/17056491.pdf

[26] F. Okino, K. Noborio, Y. Tamamoto, S. Konishi, Fusion Eng. Des. 87 (2012) 1014.

[27] T. Morisaki, S. Imagawa, A. Sagara, O. Motojima, Fusion Eng. Des. 81 (2006) 2749.

[28] M. Kondo, Y. Nakajima, Fusion Eng. Des. 88 (2013) 2556.

[29] M.A. Fütterer, J. Nucl. Mater. 283-287 (2000) 1375.

[30] S. Sharafat, N. Ghoniem, S. Zinkle, J. Nucl. Mater. 329-333 (2004) 1429.

[31] J.F. Shackelford, W. Alexander, J.S. Park, CRC Materials Science and Engineering Handbook, Second Edition (CRC Press, ISBN: 0-8493-4250-3, 1994).

[32] Y.S. Touloukian, D.P. DeWitt, Thermophysical Properties of Matter, Volume 4, Specific Heat, Metallic Elements and Alloys (IFI/Plenum, New York – Washington, 1970) 249.

[33] Z. Yuan, K. Mukai, K. Takagi and M. Ohtaka, J. Japan Inst. Metals 65 (2001) 21 (in Japanese).

[34] K. Sugiyama and K. Iguchi, Research on the fundamental process of thermal-hydraulic behaviors in severe accident –Breakup and cooling of molten material jets–, JAERI-Tech (2002) 2002-010 (in Japanese).

http://www.iaea.org/inis/collection/NCLCollectionStore/_Public/37/002/37002478.pdf

[35] R.A. Forrest and M.R. Gilbert, FISPACT-2005: User manual, UKAEA FUS (2005) 514.

http://www.ccfe.ac.uk/assets/Documents/UKAEA-FUS-514FINAL.pdf

[36] G.G. van Eden, et al., Phys. Rev. Lett. 116 (2016) 135002.

[37] J.W. Coenen, et al., Phys. Scr. T159 (2014) 014037.

[38] S. Morita, et al., Nucl. Fusion 53 (2013) 093017.

[39] M. Kobayashi, et al., Nucl. Fusion 53 (2013) 033011.

[40] Y. Nakamura, et al., Proc. of the 26th IAEA Fusion Energy Conf. (Kyoto, Japan, 17-22 October 2016) EX/P8-4.

http://www-pub.iaea.org/iaeameetings/48315/26th-IAEA-Fusion-Energy-Conference

[41] K. Shiba, A. Hishinuma, A. Tohyama and K. Masamura, Properties of Low Activation Ferritic Steel F82H IEA Heat –Interim Report of IEA Round-robin Tests (1)–, JAERI-Tech (1997) 97-038 (in Japanese).

http://www.iaea.org/inis/collection/NCLCollectionStore/_Public/28/071/28071477.pdf

[42] H. Mikami, A. Shono and H. Hiroi, Sodium Leak at Monju (I) –Cause and Consequences–, IAEA International Working Group on Fast Reactors (IWGFR/92, Technical Committee Meeting on Evaluation of Radioactive Materials Release and Sodium Fires in Fast Reactors, O-arai, Ibaraki, Japan, 11-14 Nov, 1996) pp.271-281.

http://www.iaea.org/inis/collection/NCLCollectionStore/_Public/31/044/31044820.pdf

[43] T. Goto, et al., Plasma Fusion Res 12 (2017) 1405016.

[44] Shinku Handbook (Nihon-Shinku-Gijutsu corporation, Ohm-Sha, 1992, in Japanese) pp.35-42, ISBN: 4-274-08637-2.

[45] H. Nakamura, et al., Fusion Eng. Des. 39-40 (1998) 883.

[46] J. Roth, et al., Plasma Phys. Control. Fusion 50 (2008) 103001.

[47] G. Motojima, H. Tanaka, and T. Murase, "Characteristics of the improved in-vessel cryosorption pump for the closed helical divertor in LHD", Annual Report of National Institute for Fusion Science, April 2015 – March 2016 (2016) 27.

Table 1. Comparison of the low melting point metals for the liquid metal divertor. Numerical values are basically taken from [31]. The values of T_{boil} in the bracket are taken from [28] for comparison.

	Li	Na	Ga	In	Sn	Pb	Bi
Atomic number	3	11	31	49	50	82	83
Density ρ (Mg/m^3)	0.533	0.966	5.91	7.29	7.29	11.34	9.80
Melting point T_{melt} (K)	459	371	303	430	505	601	544
Boiling point T_{boil} (K)	1,640 (1,599)	1,187	2,700	2,440	2,473 (2,781)	2,023 (2,008)	1,900
Temperature at p_{vapor} = 133.3 Pa (K)	1,023	713	1,623	(N/A)	1,883	1,243	(N/A)
Pros	Low Z Light		Low T_{melt}		Low p_{vapor} Low cost		
Cons	Water-reactive High p_{vapor}	Water-reactive High p_{vapor}	High Z Expensive	High Z Expensive	High Z	High Z Toxic Heavy	High Z Heavy
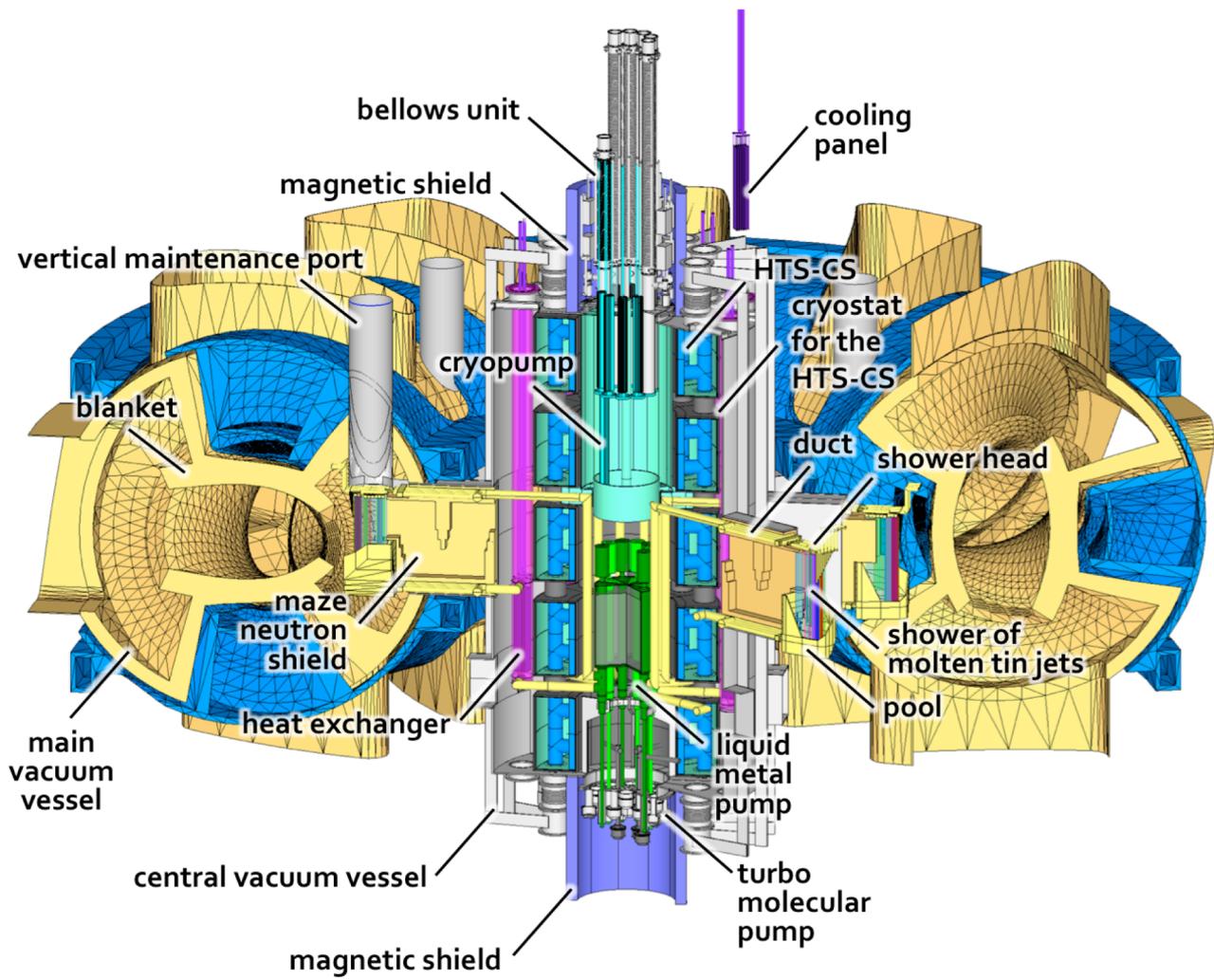
Fig 1. A bird's eye view of the FFHR-d1 equipped with the REVOLVER-D.
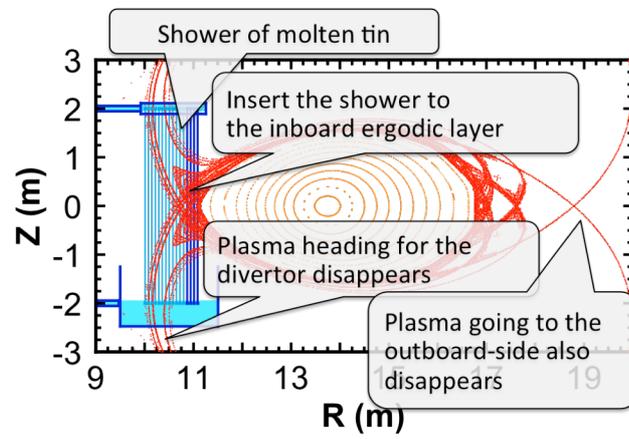
Fig. 2. A schematic view of the molten tin shower jets inserted into the inner ergodic layer.
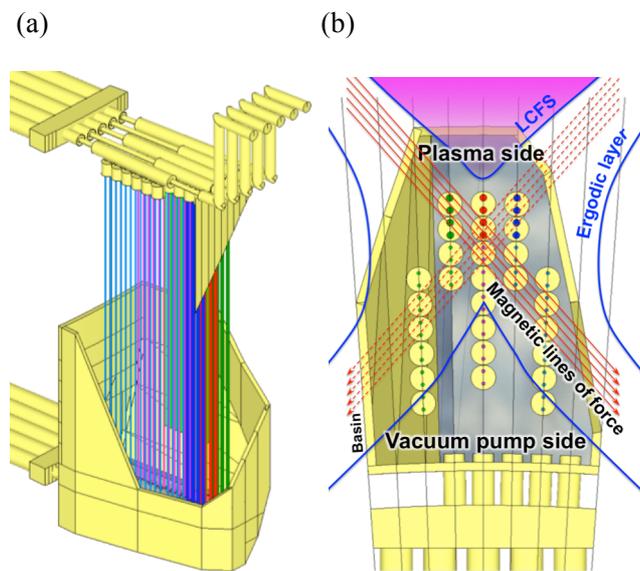
Fig. 3. (a) A bird's eye view and (b) a top view of the REVOLVER-D shower unit.
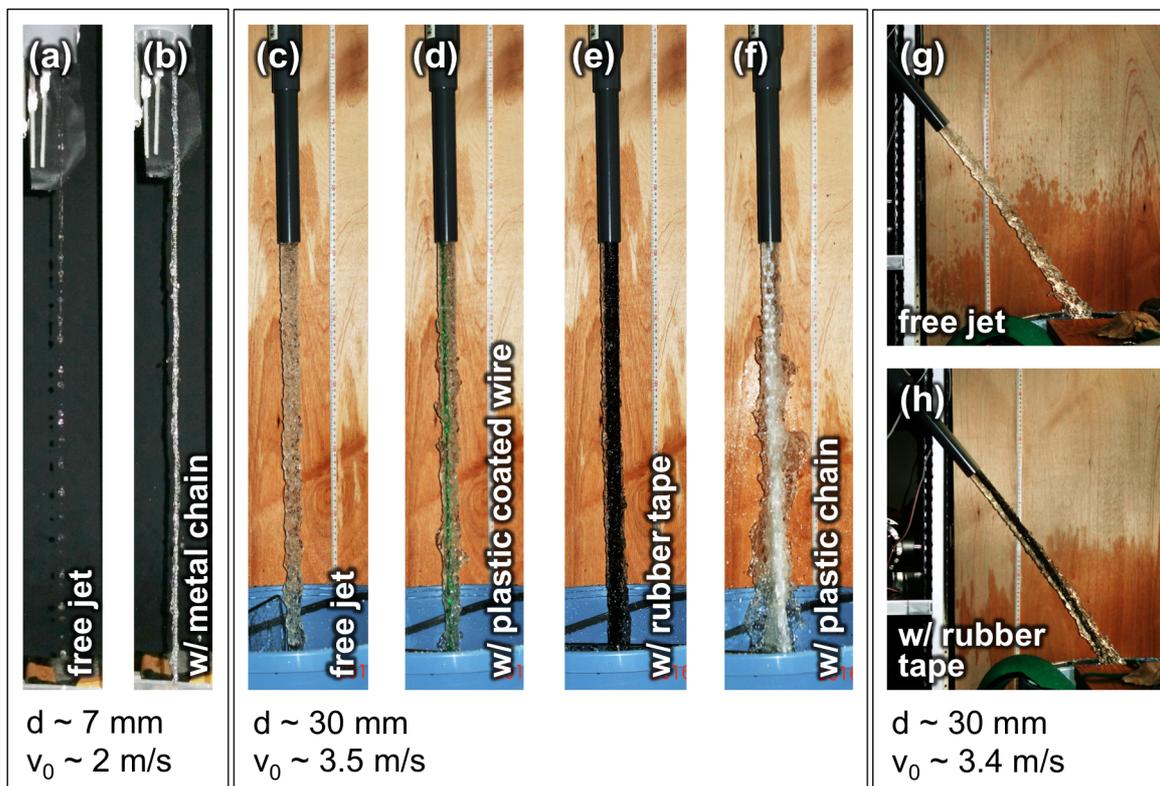
Fig 4. Various water jets issued from narrow (~ 7 mm diameter) or bold (~30 mm diameter) nozzle at slow (~2 m/s) or fast (~3.5 m/s) initial velocity. Narrow and slow jets without IFR, and with a metal chain inside are shown in (a) and (b). Bold and fast jets without IFR, with a plastic coated wire, with a rubber tape, and with a plastic chain are shown in (c) – (f). The bold and fast jets issued from a slanted nozzle without IFR, and with a rubber tape are shown in (g) and (h).
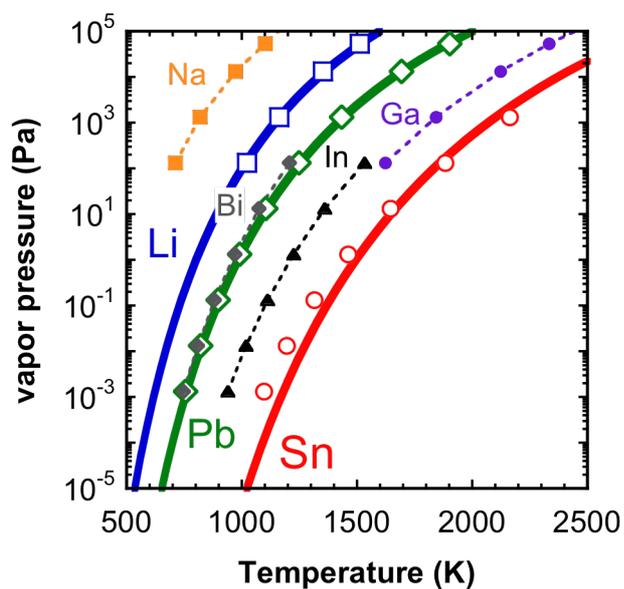
Fig. 5. The vapor pressure of low melting point materials of Li, Na, Ga, In, Sn, Pb, and Bi, as a function of the temperature. Solid curves for Li, Sn, and Pb are drawn according to the equations in [28]. Symbols denote the data in [31].
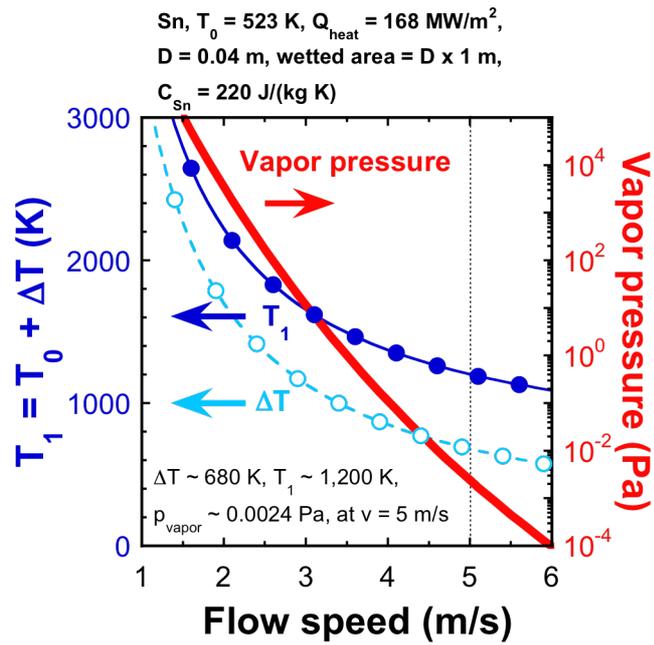
Fig. 6. The flow velocity dependence of the temperature increase, ΔT, the increased temperature, $T_1 = T_0 + \Delta T$, and the vapor pressure at T_1, in a molten tin jet of 0.04 m diameter heated by $Q_{heat} = 168$ MW/m^2 at a wetted area of 1 m length. Here, T_0 and the specific heat of tin, C_{Sn}, are assumed to be 523 K and 220 J/(kg·K), respectively.
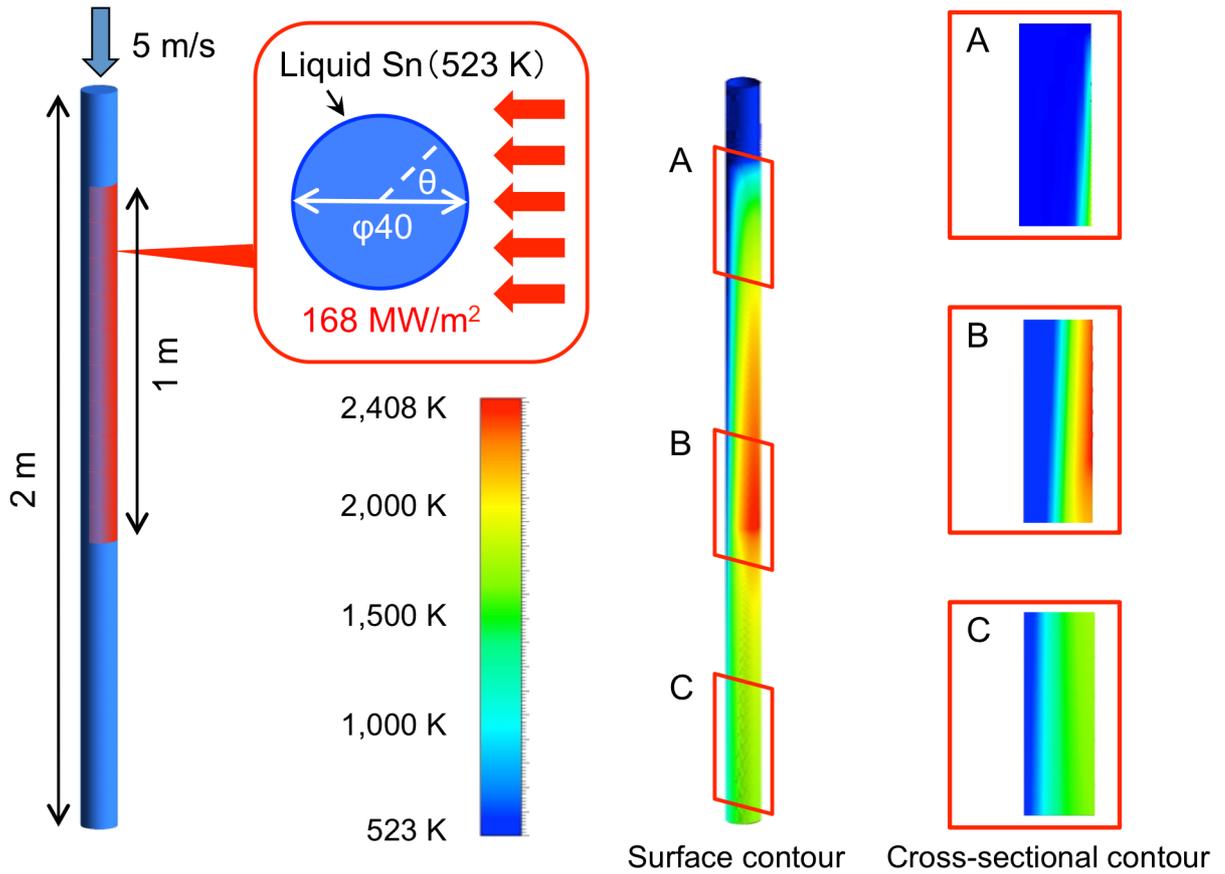
Fig 7. Examples of the simulation results given by ANSYS, where the temperature profile of a cylindrical liquid tin jet of 40 mm diameter, 2 m length, and 5 m/s constant velocity heated by 168 MW/m^2 of heat load is simulated. The heat load is applied on one side of the jet for 1 m length with a cosine profile. The initial temperature of the liquid tin jet is 523 K. The maximum surface temperature reaches 2,408 K, as seen in the surface contour plot in the center. Cross-sectional temperature profiles at the regions A, B, and C are shown in the contour plots on the right hand side. Note that no IFR is assumed and the flow is laminar in this simulation.
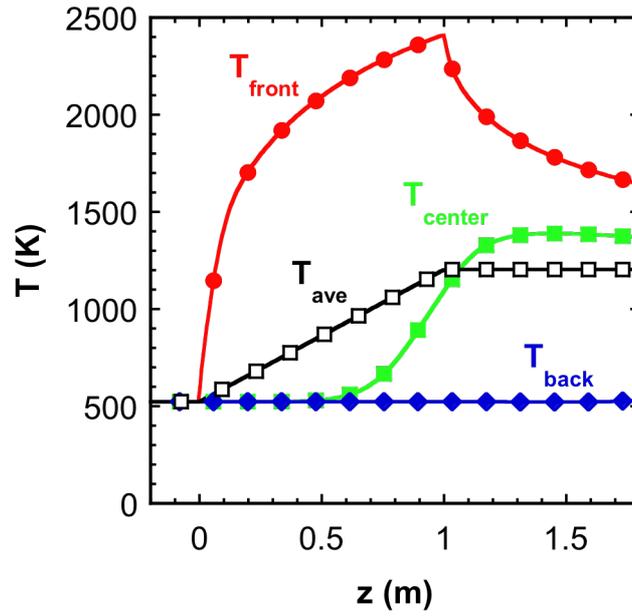
Fig. 8. The temperature profiles of the jet simulated in Fig. 7, along the downward direction of z. The temperature at the front side with respect to the heat load, T_{front}, that on the jet center, T_{center}, and that at the back side, T_{back}, are depicted by closed symbols, while the temperature averaged over the jet cross-section at z, T_{ave}, is depicted by open squares.
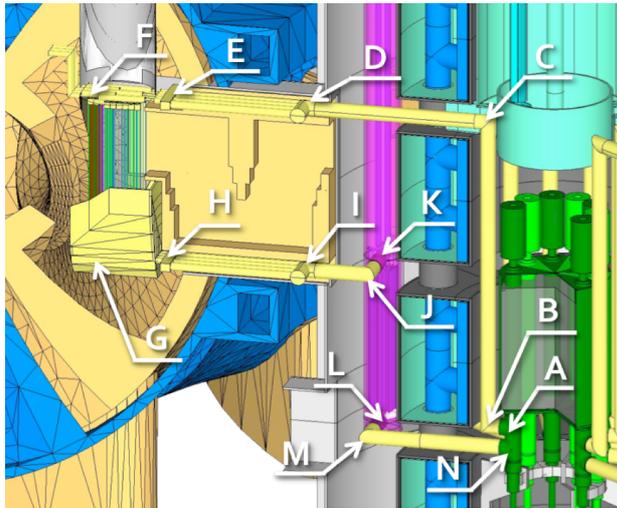
**Fig. 9.** Schematic view of the molten tin flow channel in the REVOLVER-D.
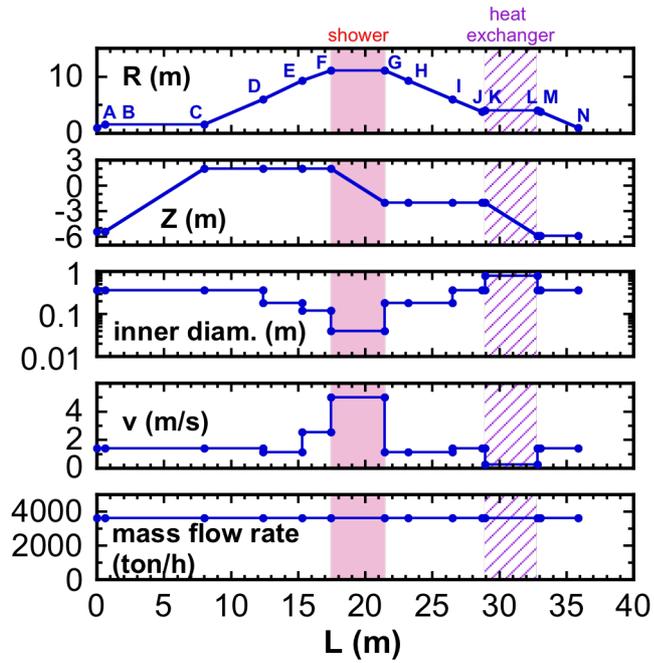
Fig. 10. Main parameters of the molten tin flow channel in the REVOLVER-D, where the radial position, R (m), the height, Z (m), the inner diameter of the duct in m, the flow velocity, v (m/s), and the mass flow rate in ton/h are shown from top to bottom. The abscissa is the channel length. Positions of A – N denoted in the top panel correspond to those in Fig. 9.
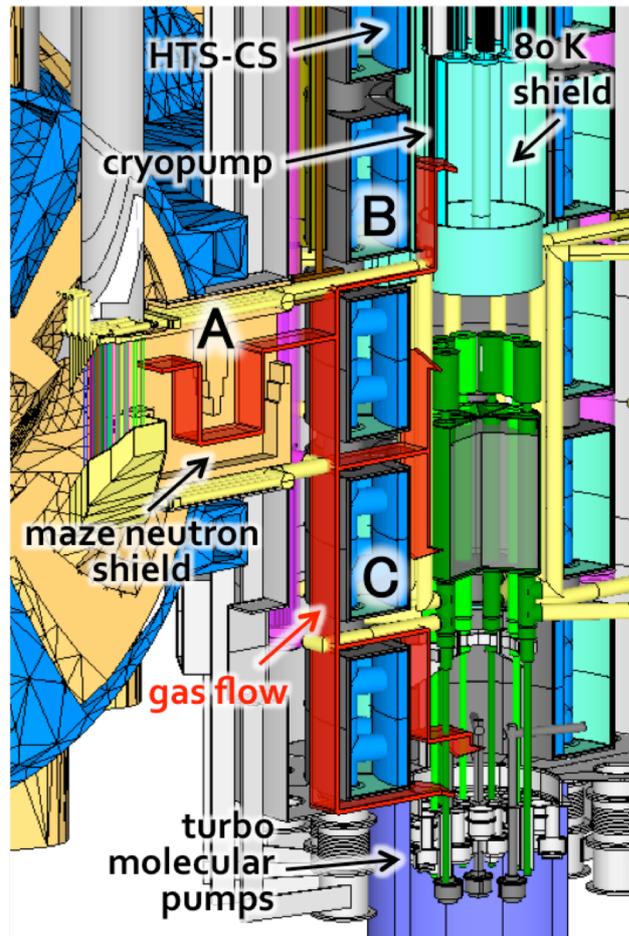
Fig. 11. Typical routes of the exhaust gas from the molten tin shower, through the maze neutron shield, to the cryopump in the 80 K thermal shield or to the TMPs in the bottom.
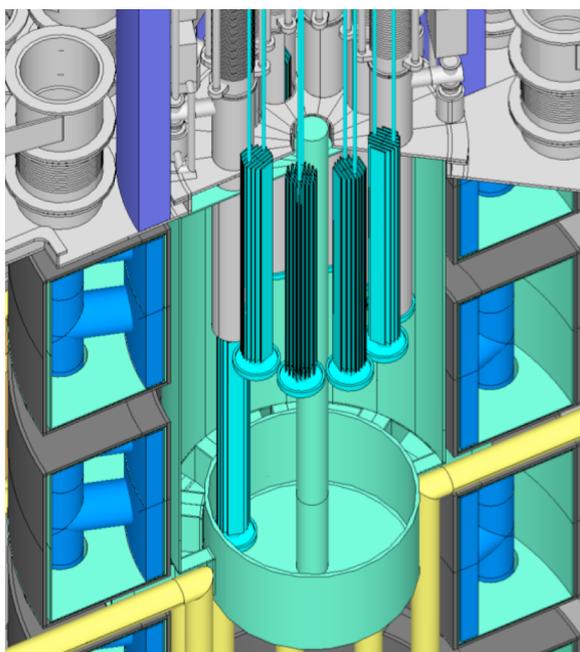
**Fig. 12.** A close-up view of the cryopanel units inside the 80 K thermal shield.
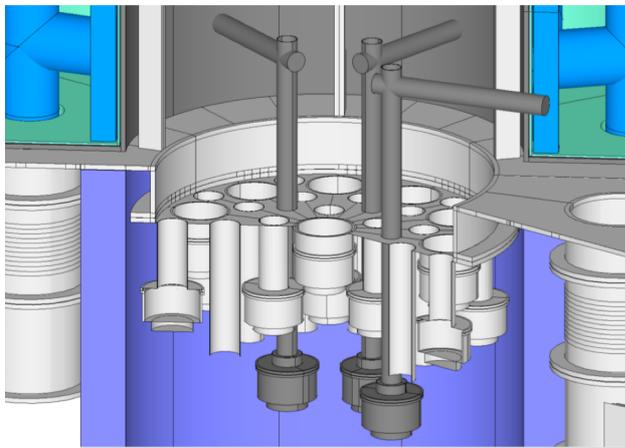
**Fig. 13.** A close-up view of the TMP assembly. Black TMPs are connected to the HTS-CS cryostat.
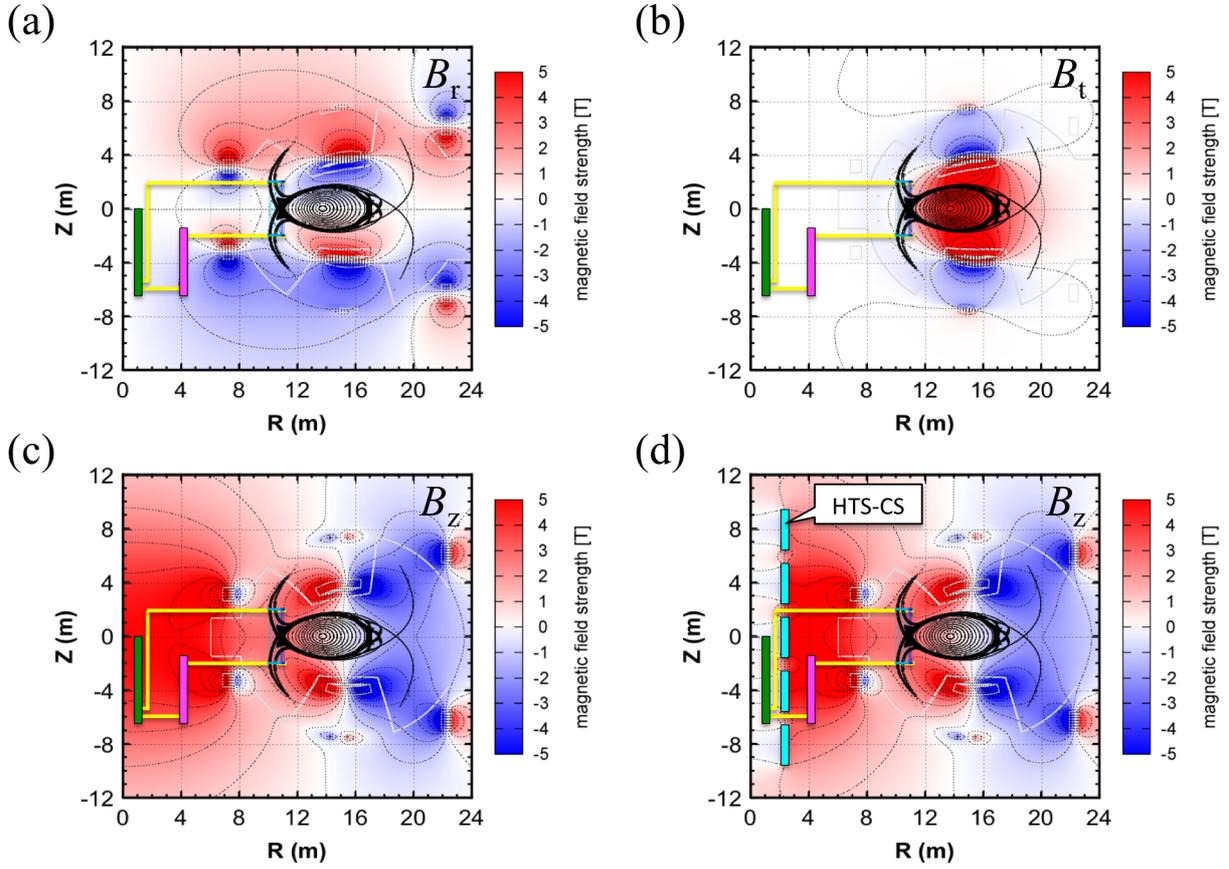
Fig. 14. Profiles of the magnetic field strength of (a) the radial field, B_r, (b) the toroidal field, B_t, (c) the vertical field, B_z, without HTS-CS and (d) the B_z with HTS-CS. In each figure, schematics of the molten tin channel and shower together with the Poincare plot of horizontally elongated magnetic surfaces are also shown.
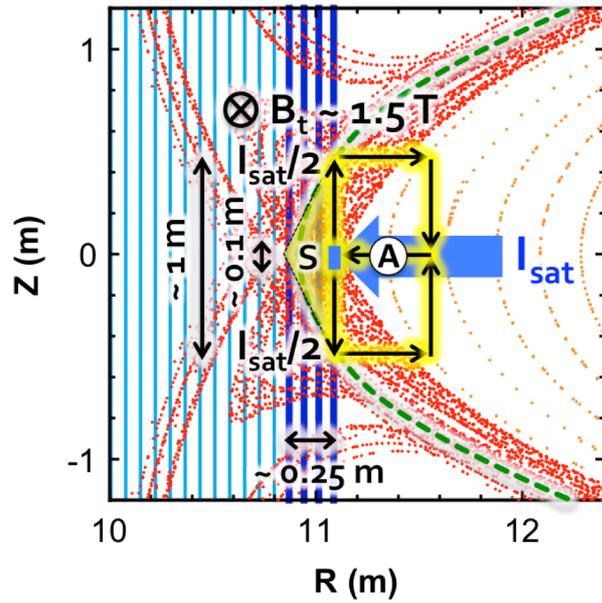
Fig. 15. An imaginary circuit where the ion saturation current is flowing through the molten tin jet. Broken curve denotes a virtual plasma boundary determined by the limiter/divertor configuration.
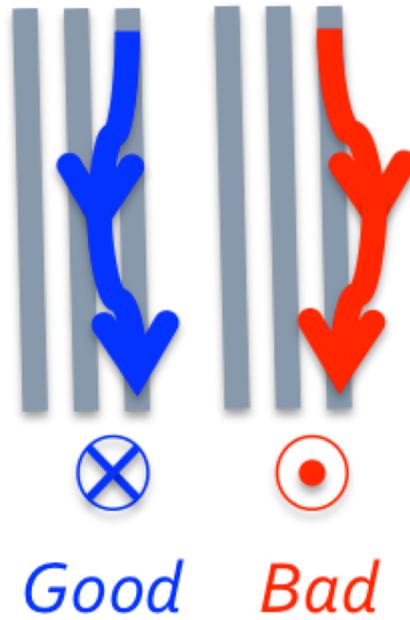
Fig. 16. Schematics of the bending jet. The bending direction depends on the directions of the magnetic field perpendicular to the jet and the electric current flowing in the jet.